How to avoid FIB-milling artefacts in micro fracture? A new geometry for interface fracture

Eloho Okotete [a], Steffen Brinckmann [b], Subin Lee [a,*], Christoph Kirchlechner [a]

[a] Institute for Applied Materials, Karlsruhe Institute of Technology, D-76344 Eggenstein-Leopoldshafen, Germany
[b] Structure and Function of Materials (IEK-2), Institute for Energy and Climate Research, Forschungszentrum Jülich, D-52428 Jülich, Germany

HIGHLIGHTS

- A new single cantilever delamination geometry is conceptualized and tested for stable crack growth in micron scale fracture experiments.
- The geometry is used to quantify interface toughness between a (Hf-Nb-Ta-Zr)C film and a silicon substrate.
- The geometry facilitates crack deflection into the interface while allowing a natural crack to grow along the interface.
- Interface toughness less susceptible to focused ion beam induced contaminants is obtained using the geometry.

GRAPHICAL ABSTRACT

A new micro cantilever geometry for interface fracture toughness
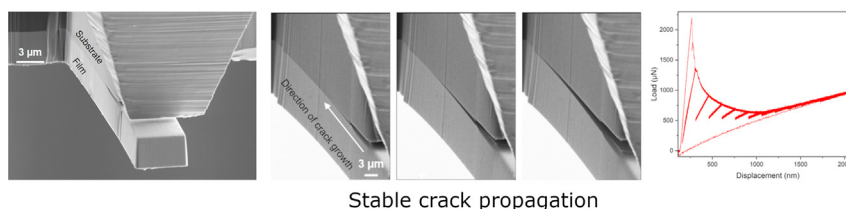
Stable crack propagation

ARTICLE INFO

ABSTRACT

Focused ion beam (FIB) based small-scale fracture studies have been well established in recent years despite the ongoing discussion of possible artefacts caused by FIB milling. Stable crack growth geometries—where the FIB-prepared notch stably propagates through the sample—have the potential to ameliorate some of the FIB-based challenges. In this work, we propose a new sample geometry for testing interface toughness at the micron scale which results in intrinsically stable crack growth. This geometry is straightforward to fabricate using established FIB-based methods and testing setups. We prove the stability of crack growth by finite element modelling and by experimentally applying the approach on a hard coating–silicon interface. We observe that even with small imperfections, the FIB-milled notch propagates towards the interface and the natural crack stably grows along the interface.

1. Introduction

As systems are miniaturized, it becomes expedient to develop tools that can reliably measure mechanical responses at comparable length scales. Small-scale mechanical testing approaches have evolved in the last decades to provide information on the deformation and fracture behaviour of material systems in small volumes [1,2]. For instance, the fracture toughness of micron and submicron sized samples are investigated using nanoindentation-based techniques [3,4] and micro fracture tests [5,6]. In such investigations samples are typically prepared by focused ion beam (FIB) milling [7,8], lithography [9], femtosecond laser machining [10], deep reactive ion etching [11], or a combination of these methods [12]. FIB enables machining of a sub-micron sized pre-notch which

---

* Corresponding author.
  E-mail address: subin.lee@kit.edu (S. Lee).

is required for localizing stress and applying standard fracture mechanics.

Simple cantilever-based geometries (rectangular, triangular and pentagonal beams) proposed by Matoy [5] and Di Maio [6] are the most prominent geometries used for micro-scale fracture studies of thin films and coatings [13–15], single interfaces [16,17] and multilayers [18,19]. However, the applicability of small-scale fracture testing for extracting bulk-like fracture properties is controversially discussed until today. A major source of concern is the presence of FIB-induced artefacts such as residual stresses due to ion implantation [20,21], and chemical interactions of Ga$^+$ including segregation at the notch tip [22,23]. Another critical drawback of FIB-based methods is the finite notch root radius which might lead to an overestimation of fracture toughness [21,24]. Fatigue pre-cracking can minimize FIB artefacts, however, it is experimentally challenging to make it and it is difficult to control the fatigue crack length in micron sized samples [25–27]. Propagating a natural crack from a FIB-milled pre-notch in a stable manner will also help limit the detrimental effect of the FIB on micro fracture experiments. This strategy of stable crack growth has been successfully shown for chevron notches in the single cantilever beam geometry [25,28]. It should be noted that milling as well as analysing the fracture toughness based on chevron notches remains challenging.

Alternative geometries such as the clamped beam bend specimens [29–32] and the double cantilever beams [33–35] have been suggested to replace the single cantilever beam. In those geometries, it is expected that the influence of the FIB damage on the fracture toughness reduces because the crack propagates in a stable manner beyond the notched region. The clamped beam which is a miniaturized three-point bend test specimen lacks analytical formulations, hence finite element method (FEM) simulations are required to extract fracture parameters for every test sample [36]. Also, FIB notches milled from the side instead of the top result in blunt and asymmetric notches. Finally, residual stresses arising e.g. from thin film growth limit the application of the clamped beam for micro fracture studies [36]. On the other hand, asymmetry is a major issue present in double cantilever beam experiments. This problem arises from (1) misalignments between the tip's central axis and the sample's central axis, (2) misalignments between the sample's surface normal and the tip's displacement axis, and (3) differences in the milled dimensions of the two beam arms [29,34]. Therefore, stable crack propagation in those geometries cannot be achieved without surmounting all the potential sources of errors, and they require substantial expertises both for FIB sample fabrication and testing. Moreover, those geometries are not suitable for thin film testing.

A simple geometry similar to the single cantilever beam with a high success rate and leads to reproducible results is needed for micro fracture studies at interfaces. The geometry should result is stable crack propagation with minimal or no influence of the FIB production. Such geometry would also find incredible use for delamination problems where mechanical failures at interfaces lead to loss of desired functionality in material systems [17,18,30].

In this study, we propose a new single cantilever delamination (SCD) geometry for the evaluation of fracture toughness of interfaces at small length scales. We apply the conceptualized geometry to measure the toughness of a hard coating–silicon interface. The geometry consists of a freestanding cantilever where a custom shaped nanoindenter tip applies a load, and a support structure which is the Si-substrate. The cantilever and the support structure have different elastic properties and are separated by a sharp interface. A notch is introduced at the interface between both parts and the load is applied to the free-standing cantilever to promote delamination fracture between the parts in fracture mode I.

2. Materials and methods

2.1. Finite element modelling

The SCD geometry was first modelled using FEM software (ABAQUS/CAE 2022, Dassault Systems, France). Fig. 1a shows a two-dimensional (2D) view of the geometry and the boundary conditions, and Fig. 1b shows the steps to obtain one sample of the SCD geometry. The 2D geometry was modelled as two materials with the modulus of the substrate kept constant and the modulus of the film varied by a factor of 3. An isotropic elastic material model was used to extract the crack driving force from the geometry. The geometry was meshed using 8-node biquadratic plane strain elements with a seam crack on the interface. The elements in the pre-crack region were biased towards the crack tip to account for the singularity at the crack tip using collapsed single node second-order quadrilateral elements with mid-side node parameter of 0.25 recommended for elastic fracture mechanics applications [37]. A contour integral approach was used to evaluate the cracks in the geometry and total of 10 contours were checked for agreement and path independence of the J-integral. Subsequently, the crack driving force, i.e. the stress intensity factor and the energy release rate, was extracted from the tenth contour around the crack tip [38]. Parametric studies were carried out to optimize the dimensions of the SCD geometry to guarantee stable crack growth.

2.2. Material system

A multi-component carbide thin film was used as a model system, which was deposited on a (100) silicon substrate by magnetron sputtering. An equimolar composition of Hf$_{25}$Nb$_{25}$Ta$_{25}$Zr$_{25}$ (Purity 99.9%, Plansee Composite Materials GmbH, Germany) and pyrolytic graphite (from Kurt J. Lesker $^®$) targets were used as source materials for the deposition. The targets were co-sputtered on the substrate at a distance of 10 cm using set ups of 0° for graphite and 45° for Hf$_{25}$Nb$_{25}$Ta$_{25}$Zr$_{25}$. Further details on the deposition procedure and analysis of the deposited film are found in Gopalan et al. [39]. The final film thickness was about 3 μm, and the equimolar composition of (Hf-Nb-Ta-Zr)C hard coating was measured by energy dispersive spectroscopy (EDS).

2.3. Cantilever preparation

The starting wafer with the thin film was mechanically cut into 2 × 2 mm pieces. The pieces were then cleaned in an ultrasonic cleaner and subjected to wet chemical etching to get free-standing films. The wet etching of silicon was carried out by placing the sample in a 30 wt.% potassium hydroxide (KOH) aqueous solution heated to 80 °C for 1 hour. Free-standing films of approximately 15 μm length were obtained from this process (see Fig. 1a and b). Subsequently, the etched samples were rinsed in distilled water, isopropanol and ethanol.

To experimentally observe the SCD geometry's fracture behaviour, 10 cantilevers with the same geometry (fabrication highlighted in Fig. 1b) were fabricated using a Ga$^+$ ion FIB source (Crossbeam 550L, Zeiss AG, Germany). The cantilevers were milled by aligning the surface normal of the free-standing film to the ion beam. Initial trenches were made using 65 nA at a dose of 50 nC/m^2 to create ample space to image the cantilever from the sides. Subsequent milling steps were as follows; a coarse step with 7 nA (dose: 35 nC/m^2), an intermediate step using 1.5 nA (dose: 30 nC/m^2), and a final polishing step using 0.7nA (dose: 25 nC/m^2). All millings were done at 30 kV. The SEM image of the FIB milled SCD geometry is presented in
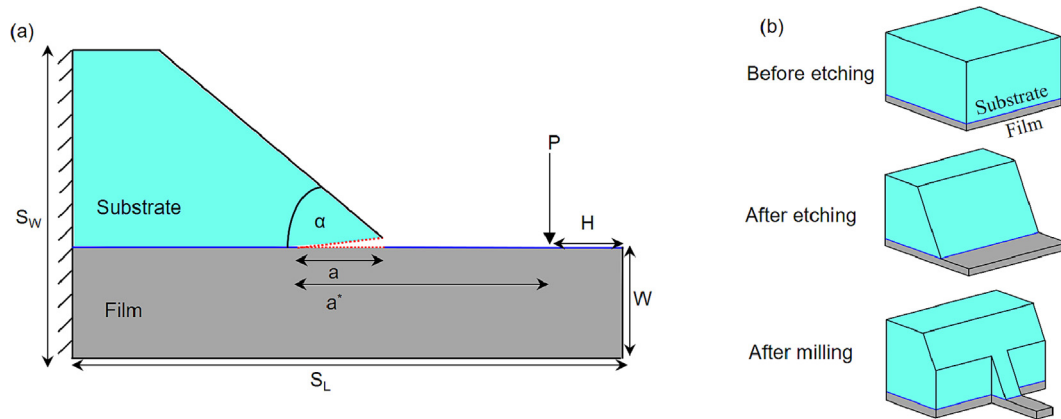
Fig. 1. (a) Sketch of the model showing applied boundary conditions for FEM simulation and the designations on the geometry are defined as follows; W—beam thickness, S_W—sample thickness, S_L—sample length, P—applied load, H—distance from loading point to the end of the cantilever, a—crack length, a^*—effective crack length (loading arm) and α—angle between substrate and film. (b) Schematic drawing showing experimental steps to prepare a cantilever with the new geometry. From the top, a sample piece from the diced wafer, geometry of the post-etching and FIB-milled geometry.

Fig. 2a. In the next step, two types of notches were milled into the cantilevers with the interface aligned parallel to the FIB source. One is a straight notch which is lying on the interface plane and extends across the cantilever's width. This notch was milled using a line pattern (current: 50 pA, dose: 2 nC/m², dwell time: 1 µs) and starts from A–B and ends at C–D (notch front) with a finite radius (Fig. 2b). The other notch is a chevron notch (Fig. 2c) which is commonly used for fracture experiments across length scales because of the ease with which a crack nucleates and the possibility of stable crack growth [28,40,41]. In our experiments, the chevron notch was milled using 100 pA (dose: 4 nC/m², dwell time: 10 µs) on the interface plane from the edges (A–D and C–E) of the cantilever sides with a point ligament at B which increases in width from B to D–E. The apex B is placed at the top of the beam instead of the center to enable accurate positioning of the apex at the center of the beam. This notch was milled with two area patterns and it required a higher optimized current than the line pattern.

2.4. Micro-fracture experiments

In situ scanning electron microscope (SEM) microcantilever bending experiments were performed in an SEM (Merlin, Zeiss AG, Germany) using a PI 89NG indenter (Hysitron, Bruker, USA). An in-house tungsten wedge tip was attached to the indenter and used for the micro-fracture experiments at a displacement rate of 10 nm/s. Partial unloading cycles at 300 nm intervals were used to monitor crack propagation during the test. The crack length was obtained from the compliance of the unloading slopes. The calculation of the crack length is described in Section 3.3.
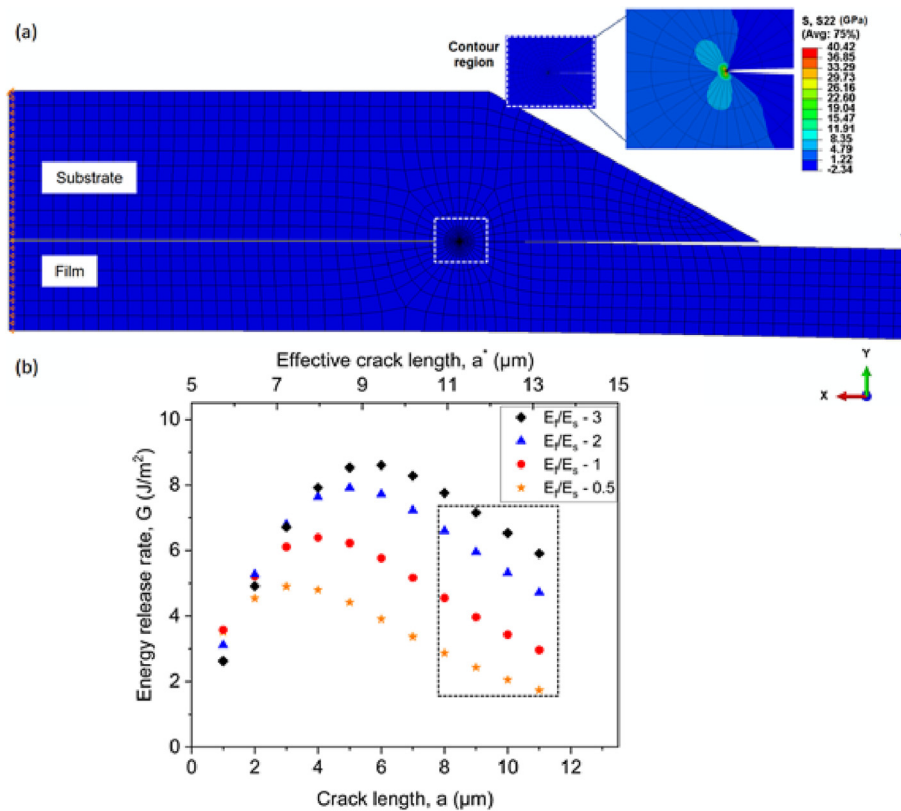
3. Results

3.1. Validation of the geometry

Fig. 3a and b show the FEM validation of the SCD geometry to assess if stable crack growth is attainable using the geometry in
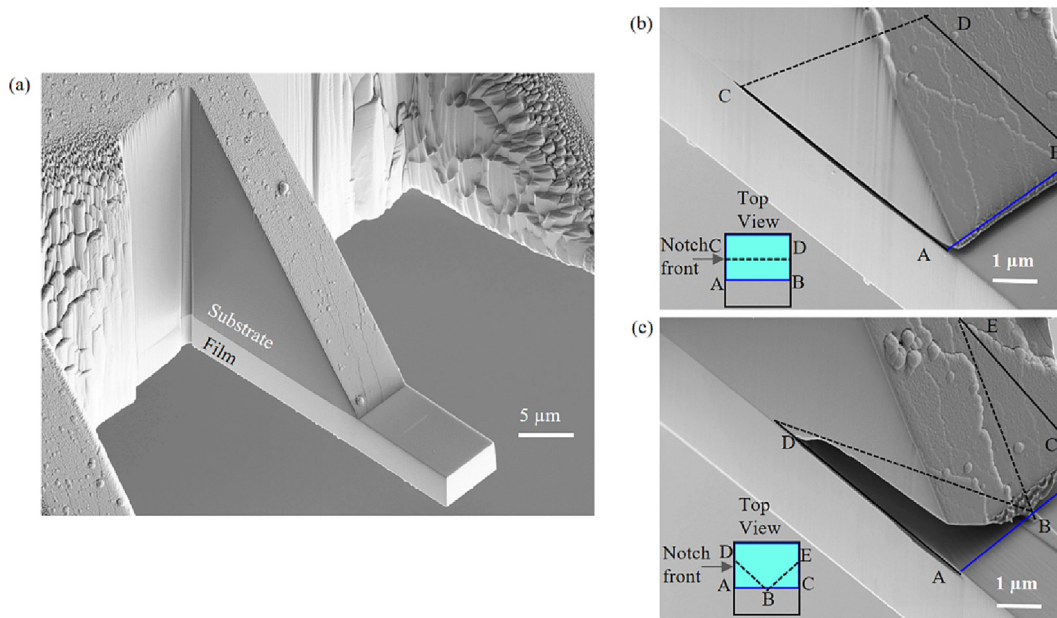
Fig. 2. (a) SEM image of the FIB fabricated cantilever highlighting the film and substrate, (b) straight notch with a sketch of the notch plane's top view, and (c) chevron notch showing the notch plane's top view.

Fig. 3. (a) A meshed geometry used for FEM calculations showing the maximum σ_{22} at the crack tip. (b) Energy release rate as a function of the crack lengths according to FEM calculations using different material property combinations for substrate (s) and film (f). The dashed window represents the region which was investigated in this study.

Fig. 1b with $W = 0.375\ S_W$. In Fig. 3a, the meshed geometry showing the contour region and the maximum stresses at the crack tip is seen for a calculation with $E_f\ /\ E_s$ ratio of 1. It is found that the energy release rate first increases with crack length for different combinations of Young's modulus in Fig. 3b. Nevertheless, the energy release rate always decreases for cracks longer than 6 μm. This observation implies a reduction in the crack driving force when the crack length increases and therefore one expects stable crack growth in the subsequent *in situ* SEM testing. The reduction in the driving force is attributed to the increase in compliance of the longer cantilever at longer crack lengths if the cantilever is displacement-controlled loaded. The region of stable crack growth is indicated with the dashed box in Fig. 3b. The present experiments probe this window.

3.2. Stable crack growth during in situ SEM testing

Fig. 4 shows representative results from a cantilever with a straight notch. The setup of the cantilever and the tungsten wedge tip is presented in Fig. 4a. To measure the stiffness changes from the unloading parts of the load–displacement curve, the sample is partially unloaded every 300 nm. In Fig. 4b, the initial loading region is observed with a maximum load of 2200 μN as marked by "c". Beyond point c, an initial load drop is observed which indicates the start of crack propagation (see Supplementary Video 1). As the load continues to drop between Points c and d, we observe a deflection of the notch (pre-notch introduced from FIB) onto the interface plane in Fig. 4d. Points e–h and corresponding SEM images (Fig. 4e–h) show the crack propagating in a stable manner along the interface as indicated by the arrows. Similar stable crack growth seen in Fig. 4 is observed in the other samples with straight notches (see Supplementary Fig. S1).

In the samples with chevron notches, a short ligament (point B in Fig. 2c) fails first and the crack propagates through the triangular chevron shape till the point where the crack became parallel to the interface plane (D–E). At that point, the behaviour of the chevron notch samples become identical to the straight notched samples, and a similar load–displacement profile as Fig. 4 and crack opening behaviour are observed (see Supplementary Fig. S2).

In all these experiments, there is an absence of catastrophic failures in any of the cantilever beams which indicates that the crack is stable when using the new geometry. This observation matches well with the FEM calculations (Fig. 3) which pointed to an intrinsically stable geometry for micro fracture experiments, particularly for interfaces. The crack length estimation from the unloading compliance slopes and SEM images is discussed in the next Section (3.3).

3.3. Quantification of interface toughness

The compliance from the individual unloading slopes (C_M) in Fig. 4b is used to calculate the crack length by applying Bernoulli theory (Eq. (1)) assuming a cantilever of length a^* (Fig. 1) with a clamped end at the crack tip. This assumption represents an upper-bound of the crack length.

$$a^* = \left(\frac{C_M E_f B W^3}{4} \right)^{1/3} \tag{1}$$

where a^*– effective crack length, C_M — compliance from unloading slope, E_f — elastic modulus of film, W — beam thickness, and B — beam width.

However, external compliances are present and need to be corrected. We summarize these compliances into one frame compli-
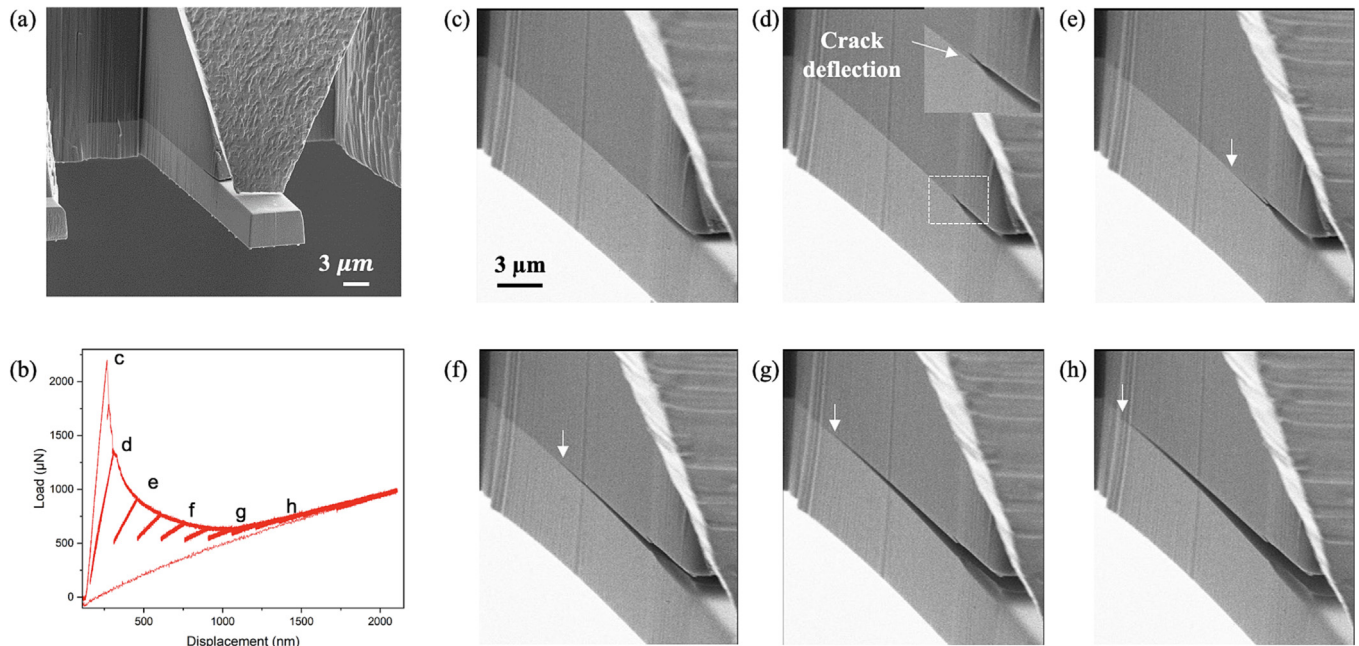
Fig. 4. (a) Setup of cantilever and indenter tip for *in situ* testing, (b) load vs displacement plots from the experimental investigation showing partial unloading segments during the test. (c – h): SEM images showing stages of crack deflection and growth during the test.

ance (C_F) and calculate it using three methods. Firstly, we calculated the frame compliance (C_{F-C}) by subtracting the measured compliance of the initial loading slope (C_0) from the compliance of the beam (C_B) calculated from Eq. (2). Secondly, we directly measured the frame compliance by applying a normal force on the same macro sample in a region close to the cantilevers (C_{F-M}). This method is necessary because standard compliance correction methods would not work for the custom-made wedge tip, the tapered geometry of our sample obtained from the etching process and the different sample mounting of the potential fused silica reference (see Supplementary Fig. S3). Finally, we simplify the first approach and just take the compliance of the initial loading slope (C_0) as the frame compliance C_{F-0} and thereby evaluate the crack advance from its initial position. C_F obtained from all three methods is subsequently compared and used to correct all measured compliances C_M^i, where i indicates the unloading sequence. The corrected compliance (C_M^* in Eq. (3) is substituted into Eq. (1) to obtain the corrected crack effective length (a^*). The crack lengths from the uncorrected and corrected data are shown in Fig. 5a.

$$C_B = \frac{4a^{3*}}{E_f BW^3} \quad (2)$$

$$C_M^* = C_M - C_F, with(C_F = C_{F-C}\, or\, C_{F-M}\, or\, C_{F-0}) \quad (3)$$

For comparison, the crack length is also directly measured from *in situ* SEM frames at points corresponding to the unloading as plotted in Fig. 5a. The crack length (measured and calculated) increases with displacement irrespective of the determination method. Fig. 5a shows that the crack lengths measured from SEM images do not exactly match the ones based on the unloading stiffness, however the differences in the crack lengths corrected by different compliance correction methods are only marginally different (seen in Fig. 5b) especially at larger displacementssuggesting all methods are equally suited to correct the measured compliance (C_M).

To further corroborate this assertion, the compliance-corrected and SEM-measured crack lengths from Fig. 5a are plotted against critical energy release rate, G_c, calculated using the area method [42,43] (Fig. 6). In the area method, G_c (G_{c_H}) is obtained by dividing
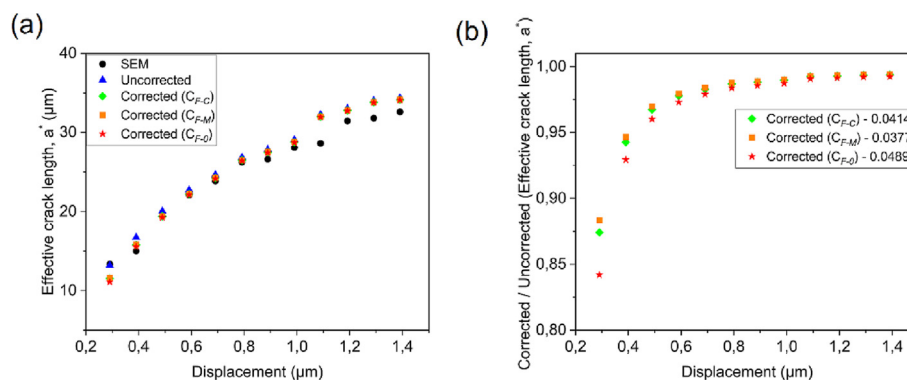
Fig. 5. (a) Crack length from SEM post-mortem images, corrected unloading slopes' compliances, and uncorrected unloading slopes' compliance. (b) Normalized corrected crack lengths showing different methods used for correcting the external compliance contribution.
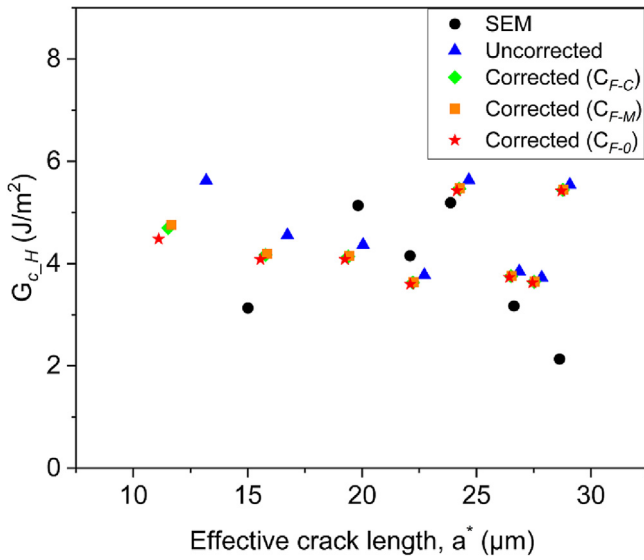
Fig. 6. Changes in critical energy release rate, G_{c_H}, calculated by area method using crack length presented in Fig. 5a.

the energy loss (the area between the loading and unloading curves) due to crack growth for example Fig. 4b by the area of the crack (Eq. (4). G_{c_H} can be expressed as,

$$G_{c\_H} = \frac{1}{B}\frac{\Delta H}{\Delta a} \qquad (4)$$

where ΔH is the energy for crack growth, B is width of the cantilever, and Δa is the crack extension.

It is found that G_{c_H} remains nearly constant with increasing crack length for SEM-measured, uncorrected and compliance-corrected data (Fig. 6) with little scatter in the results. Since the result in Fig. 6 do not show any dependence on the crack length correction method, C_{F-C} is chosen to correct the crack length in the chevron notched samples. Using this C_{F-C} corrected- crack length, we calculate G_{c_H} for all samples. We subsequently conducted an error propagation analysis based on the mechanical measurements for the results in Fig. 6 to ascertain the certainty of the data presented. Details of the error propagation analysis and a plot of the uncertainty measured are in the attached supplementary material (see Supplementary Fig. S4).

Lastly, we compare the G_c of the interface measured from cantilevers with the two notch shapes, straight and chevron notches (Fig. 7a). Firstly, we observe in Fig. 7b that the energy dissipated as the crack grows is similar for both notch types. However, there

are initial higher values of G_{c_H} for the chevron notched samples in Fig. 7a at smaller crack lengths, followed a gradual decrease at longer crack lengths. We also see scatter in G_{c_H} some samples which could be from some inaccuracies that may have been introduced from crack length estimation. It suggests that regardless of the notch shape, we observe stable crack growth for an extended period using the new geometry and that the crack growth is beyond the region which was influenced by most FIB-based artefacts to the fracture properties. Moreover, as the crack propagates, the curves converge to similar G_c because we get a crack front parallel to the interface in all samples. To summarize, these results infer that the crack stability in this geometry is insensitive to notch type and changes in the cantilever's dimensions.

4. Discussion

4.1. Stable crack growth

In materials with constant resistance to crack propagation R, a crack propagates in a catastrophic manner, so-called unstable growth, if the crack driving force, G, is increasing with crack length. However, if G is decreasing with increasing the crack length a, the crack will extend in a controlled fashion (stable growth) and will stop growing unless the external load is increased [44–46].

In recent years, several studies have tried to demonstrate stable fracture experiments using geometries such as clamped beam or using different notch types like chevron notches [29,41,47]. This stable crack propagation is particularly needed to extract intrinsic properties of interfaces at small length scales in which sample fabrication techniques, like FIB milling, can have an influence on the apparent fracture toughness [34,48,49]. If the crack stably propagates, it is also possible to monitor the changes in fracture toughness as a crack propagates. In our study, we see a reducing G with increasing crack length, a, by using FEM calculations indicating that a growing crack will be stable if the geometry satisfies certain conditions ($\frac{dG}{da} \leq \frac{dR}{da}$). The crack stability is further confirmed by the observation that the off-axis pre-notch results into the crack deflection onto a favourable interface crack-path.

4.2. Crack deflection: FIB pre-notch vs natural crack

The elastic property mismatch between the materials adjoining an interface leads always to a mixed mode loading at the interface crack tip irrespective of the loading of the far-field stresses [50–53]. This mixed mode loading, the interface chemistry and interface morphology determine the crack propagation direction in layered materials [54–56]. If the interface offers the path of least resistance with respect to the resolved driving force along that
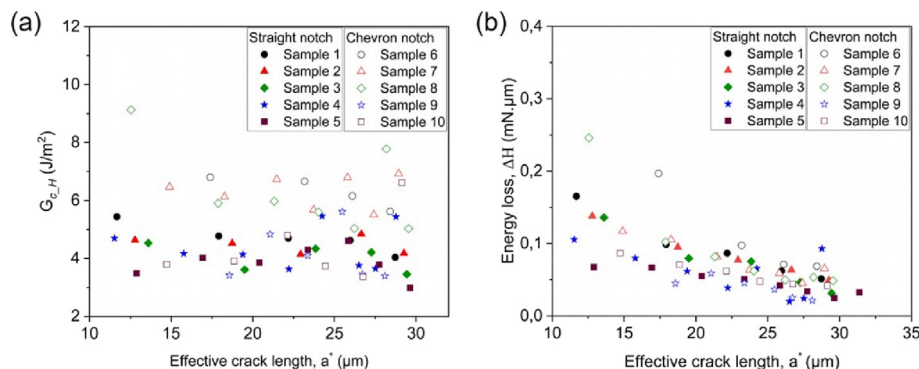

Fig. 7. (a) Interface toughness G_c, for cantilevers with two notch types, calculated by area method from the experimental data. (b) Energy loss (ΔH) as crack grows, for cantilevers with two notch types, calculated between the loading and unloading curves in Fig. 4b.

plane, a crack will grow along the interface irrespective of the mixed mode loading. In such cases, the driving force (the energy release rate) to propagate a crack in the adjacent materials is lower than the fracture resistance (fracture energy for the creation of new surfaces) in the adjacent materials; however the driving force to propagate a crack in the interface is higher than the interfacial fracture resistance [57,58]. Hence, a pre-existing near-interface crack will deflect into the interface and grow along the interface when the condition in Eq. (5) is satisfied and if the interface is the path of least resistance.

$$\frac{R_i}{R_b} < \frac{G_i}{G_b} \qquad (5)$$

where R_i is the interface fracture energy, R_b is the bulk fracture energy of the materials, G_i is the strain energy release rate of the interface and G_b is the strain energy release rate of the bulk.

In the present study, the FIB-milled notches near the interface develop into natural cracks which grow along the interfaces. This deflection occurs after the slightly misaligned FIB-notch grows a few micrometers (Fig. 8b). Fig. 8b shows that the notch front is actually C*–D* not C–D (Fig. 8a). The connection C–D is a FIB arte-fact and was the only part that was visible before the *in situ* experiments. The hidden true notch front C*–D* grows to critical length and then deflects onto the interface. At this deflection, a natural sharp crack is formed at the interface which is required for an accurate evaluation of the fracture toughness [59]. This natural crack is free of FIB artefacts like residual stresses due to ion implantation, chemical interactions of Ga⁺ including segregation and finite notch root radius. With the formation of the natural crack, we obtained a crack with an ideally uniform width on the interface plane. This observation shows that this fracture geometry eliminates errors arising from over-fibbing which was one motiva-tion for using bridge notches [5].

In cantilevers with a chevron notch, the crack fails at the chev-ron apex. However, the crack deflection into or off the center-plane cannot be imaged by SEM during early stages of the experiment because the chevron apex is shadowed by the pre-crack. The grow-ing crack is only visible from the cantilever sides after the crack has passed the triangular chevron shape. Hence, early crack growth is difficult to analyze and verify. This could also contribute to the high G_{c_H} in chevron sample at short crack length–from the apex of the chevron to the end of the triangular section.

4.3. Interface toughness

We observe that the interface toughness–the critical energy release rate of the interface (G_c) – is higher when the crack is within a few microns of the notch root with a finite root radius. As our natural crack grows beyond the region near the pre-notch, G_c reduces and plateaus with longer cracks (Figs. 6 and 7). This

toughness evolution implies that the toughness in the plateau region is representative of the material property probed using the SCD geometry. Hence, the present geometry serves as a useful method for quantitative analysis of interfaces in both functional and structural systems at small-length scales. In this case, we are able to extract the true toughness of the (Hf-Nb-Ta-Zr)C film/sili-con interface.

The G_c recorded for the interface in this study is compared to the toughness of the bulk materials since a deflected natural crack was propagated during testing. For Eq. (5) to be satisfied, we expect a lower G_c compared to the fracture energies of the bulk materials. In Fig. 7a, we see that G_{c_H} plateaus at a range between 3 and 6 J/m² and we compare these values presented in our study to cleavage energies of 3––12 J/m² reported for different planes of transition metal carbides by Yu *et al.* [60]. For the silicon substrate, several studies using experiments and density functional theory (DFT) cal-culations have reported cleavage energies of silicon to be in the range of 3.0 – 4.0 J/m² for (110) [61–65], 2.2 – 3.6 J/m² (111) [61,62,65,66], 2.82 – 4.78 J/m² (100) [65] planes, respectively. These cleavage energies of the bulk material systems represent the resistance offered by these systems to crack propagation. We see that the G_c of the interface is lower than the cleavage energy of the (Hf-Nb-Ta-Zr)C film. Hence, the driving force for interface delamination is higher than the driving force for film failure for a near-interface crack.

For Si, the (100) plane is the plane oriented perpendicular to the loading direction and we would expect deflection into this plane compared to the usual low-energy cleavage planes. The cleavage energy of Si (100) is within the upper domain of the interface toughness that was determined in this study, which could imply a possible deflection of the crack from the interface into a parallel Si plane. However, a native oxide of a few nanometers is present on the surface of the silicon substrate. This silicon oxide has fracture energies in the range of 6.2 – 9 J/m² [5,67] from theo-retical and experimental data. Also showing that the driving force for interface delamination is higher than the driving force for frac-ture for silicon fracture assuming negligible geometry contribu-tions when the milled notch is near the interface.

These comparisons have shown the data obtained for the inter-face toughness using the single cantilever beam geometry are within the expected range to justify i) crack deflection into the interface we see in our experiments and ii) crack path along the interface which enables us to grow a stable crack beyond the FIB artefact influenced region of the cantilever.

4.4. Application of geometry to other systems

Within this work, the SCD geometry has been specifically applied to an interface with adjoining brittle materials where the driving force for interface failure supersedes the driving force for
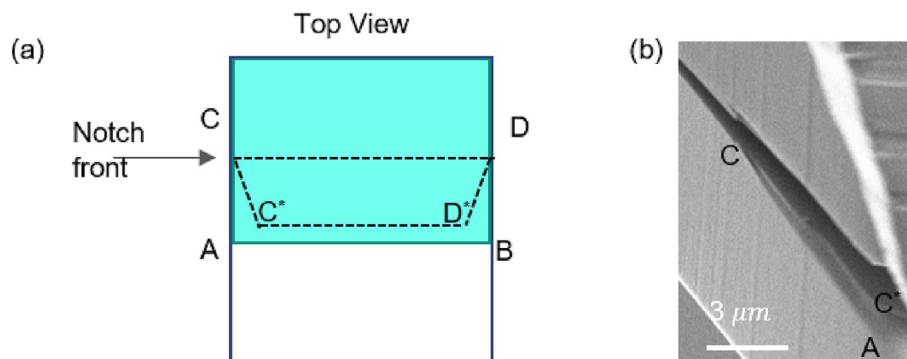

Fig. 8. (a) Schematic of a fibbed notch plane, the assumed plane (ACDB) vs the actual plane (AC*D*B). (b) SEM image showing crack propagation on the AC*D*B notch plane and the deflection into the interface plane at point C.

failure of the adjoining bulk materials. To determine the range of materials systems where this geometry can be used to measure interface toughness, we carried out several 2D FEM simulations following the procedure described in Section 2.1 with a w/S_w ratio of 0.1 similar to the geometry used in the experiments. In these calculations, we observe that the geometry gets stable irrespective of the moduli differences (see Supplementary Fig. S5). However, whether or not interface delamination is the dominant failure mechanisms depends on several additional aspects, for example, the fracture toughness of the film and the substrate, plastic deformation, possible anisotropy, film thickness and certainly many more. Even the interface toughness itself can affect whether or not the crack will propagate along the interface in our SCD geometry. Having said that, we do not think that this geometry would cause delamination in systems with a ductile film on a brittle substrate. Hence, the elastic modulus alone is not sufficient to predict the application range of the SCD geometry. Therefore, more investigation is required to give the exact range where this technique breaks down. At the time of this investigation, this study has shown that the SCD geometry promotes stable crack growth in brittle systems with weak interfaces.

5. Conclusion

A new single cantilever delamination geometry for stable crack growth was conceptualized and tested. FEM simulations and experimental results show that a crack present in the SCD geometry is stable. Stable crack propagation was achieved in all experiments in the presence of a natural crack that propagated from a FIB-milled straight and chevron notches avoiding classical problems of FIB-based fracture mechanics, i.e. blunt notch, Ga$^+$ damage. We also prove that it is possible to measure the fracture properties of individual interfaces in functional material systems using the SCD geometry. The fracture toughness G_{c_H} of the interface between a (Hf-Nb-Ta-Zr)C film and a silicon substrate was in a range of 3 – 6 J/m². These values are lower than the fracture toughness of the film and within the toughness of the Si-substrate making the interface the preferred path for crack growth due to the SCD geometry.

Data availability

Data will be made available on request.

Declaration of Competing Interest

The authors declare that they have no known competing financial interests or personal relationships that could have appeared to influence the work reported in this paper.

Acknowledgement

Appendix A. Supplementary data

Supplementary data to this article can be found online at https://doi.org/10.1016/j.matdes.2023.112134.

References

[1] G. Dehm, B.N. Jaya, R. Raghavan, C. Kirchlechner, Overview on micro- and nanomechanical testing: New insights in interface plasticity and fracture at small length scales, Acta Mater. 142 (2018) 248–282.

[2] B.N. Jaya, Z. Alam, Small-scale mechanical testing of materilas, Curr. Sci. 105 (2013) 1073–1099.

[3] W.C. Oliver, G.M. Pharr, An improved technique for determining hardness and elastic modulus using load an ddisplacement sensing identation experiments, J. Mater. Res. 7 (1992) 1564–1583.

[4] G.M. Pharr, Measurement of mechanical properties by ultra-low load indentation, Mater. Sci. Eng. A 253 (1-2) (1998) 151–159.

[5] K. Matoy, H. Schönherr, T. Detzel, T. Schöberl, R. Pippan, C. Motz, G. Dehm, A comparative micro-cantilever study of the mechanical behavior of silicon based passivation films, Thin Solid Films 518 (1) (2009) 247–256.

[6] D. Di Maio, S.G. Roberts, Measuring fracture toughness of coatings using focused-ion-beam-machined microbeams, J. Mater. Res. 20 (2) (2005) 299–302.

[7] M.W. Phaneuf, Applications of focused ion beam microscopy to materials science specimens, Micron 30 (3) (1999) 277–288.

[8] C.A. Volkert, A.M. Minor, Focused Ion Beam Micromachining, MRS Bull. 32 (2007) 389–399.

[9] T. Connolley, P.E. Mchugh, M. Bruzzi, A review of deformation and fatigue of metals at small size scales, Fatigue Fract. Eng. Mater. Struct. 28 (12) (2005) 1119–1152.

[10] M.J. Pfeifenberger, M. Mangang, S. Wurster, J. Reiser, A. Hohenwarter, W. Pfleging, D. Kiener, R. Pippan, The use of femtosecond laser ablation as a novel tool for rapid micro-mechanical sample preparation, Mater. Des. 121 (2017) 109–118.

[11] J.C. Rich, David Boyd, Christenson, Deep Reactive Ion etching Process and microelectromechanical devices formed thereby, US 7077007 B2, 2006

[12] S. Wurster, C. Motz, M. Jenko, R. Pippan, Micrometer-sized specimen preparation based on ion slicing technique, Adv. Eng. Mater. 12 (1-2) (2010) 61–64.

[13] A. Riedl, R. Daniel, M. Stefenelli, T. Schöberl, O. Kolednik, C. Mitterer, J. Keckes, A novel approach for determining fracture toughness of hard coatings on the micrometer scale, Scr. Mater. 67 (7-8) (2012) 708–711.

[14] B. Völker, B. Stelzer, S. Mráz, H. Rueß, R. Sahu, C. Kirchlechner, G. Dehm, J.M. Schneider, On the fracture behavior of Cr2AlC coatings, Mater. Des. 206 (2021) 109757.

[15] S. Massl, W. Thomma, J. Keckes, R. Pippan, Investigation of fracture properties of magnetron-sputtered TiN films by means of a FIB-based cantilever bending technique, Acta Mater. 57 (6) (2009) 1768–1776.

[16] J. Schaufler, C. Schmid, K. Durst, M. Göken, Determination of the interfacial strength and fracture toughness of a-C: H coatings by in-situ microcantilever bending, Thin Solid Films 522 (2012) 480–484.

[17] H. Hirakata, T. Kitamura, T. Kusano, Pre-cracking technique for fracture mechanics experiments along interface between thin film and substrate, Eng. Fract. Mech. 72 (12) (2005) 1892–1904.

[18] R. Konetschnik, R. Daniel, R. Brunner, D. Kiener, Selective interface toughness measurements of layered thin films, AIP Adv. 7 (3) (2017) 035307.

[19] M. Alfreider, J. Zechner, D. Kiener, Addressing Fracture Properties of Individual Constituents Within a Cu-WTi-SiOx-Si Multilayer, JOM 72 (12) (2020) 4551–4558.

[20] C.M. Lauener, L. Petho, M. Chen, Y. Xiao, J. Michler, J.M. Wheeler, Fracture of Silicon: Influence of rate, positioning accuracy, FIB machining, and elevated temperatures on toughness measured by pillar indentation splitting, Mater. Des. 142 (2018) 340–349.

[21] A.D. Norton, S. Falco, N. Young, J. Severs, R.I. Todd, Microcantilever investigation of fracture toughness and subcritical crack growth on the scale of the microstructure in Al2O3, J. Eur. Ceram. Soc. 35 (16) (2015) 4521–4533.

[22] J.P. Best, J. Zechner, J.M. Wheeler, R. Schoeppner, M. Morstein, J. Michler, Small-scale fracture toughness of ceramic thin films: the effects of specimen geometry, ion beam notching and high temperature on chromium nitride toughness evaluation, Phil. Mag. 96 (2016) 3552–3569.

[23] J.P. Best, J. Zechner, I. Shorubalko, J.V. Oboňa, J. Wehrs, M. Morstein, J. Michler, A comparison of three different notching ions for small-scale fracture toughness measurement, Scr. Mater. 112 (2016) 71–74.

[24] S. Wurster, C. Motz, R. Pippan, Characterization of the fracture toughness of micro-sized tungsten single crystal notched specimens, Phil. Mag. 92 (14) (2012) 1803–1825.

[25] M.G. Mueller, V. Pejchal, G. Žagar, A. Singh, M. Cantoni, A. Mortensen, Fracture toughness testing of nanocrystalline alumina and fused quartz using chevron-notched microbeams, Acta Mater. 86 (2015) 385–395.

[26] K. Takashima, Y. Higo, Fatigue and fracture of a Ni-P amorphous alloy thin film on the micrometer scale, Fatigue Fract. Eng. Mater. Struct. 28 (8) (2005) 703–710.

[27] P. Grünewald, J. Rauber, M. Marx, C. Motz, F. Schaefer, Fatigue crack growth in micro specimens as a tool to measure crack–microstructure interactions, Fatigue Fract. Eng. Mater. Struct. 43 (12) (2020) 3037–3049.

[28] G. Žagar, V. Pejchal, M.G. Mueller, L. Michelet, A. Mortensen, Fracture toughness measurement in fused quartz using triangular chevron-notched micro-cantilevers, Scr. Mater. 112 (2016) 132–135.

[29] B.N. Jaya, V. Jayaram, Crack stability in edge-notched clamped beam specimens: Modeling and experiments, Int. J. Fract. 188 (2) (2014) 213–228.

[30] J.L. Mead, M. Lu, H. Huang, Inducing stable interfacial delamination in a multilayer system by four-point bending of microbridges, Surf. Coatings Technol. 320 (2017) 478–482.

[31] Y. Hu, J.-H. Huang, J.-M. Zuo, In situ characterization of fracture toughness and dynamics of nanocrystalline titanium nitride films, J. Mater. Res. 31 (3) (2016) 370–379.

[32] N. Jaya B, V. Jayaram, S.K. Biswas, A new method for fracture toughness determination of graded (Pt, Ni)Al bond coats by microbeam bend tests, Phil. Mag. 92 (25-27) (2012) 3326–3345.

[33] S. Liu, J.M. Wheeler, P.R. Howie, X.T. Zeng, J. Michler, W.J. Clegg, Measuring the fracture resistance of hard coatings, Appl. Phys. Lett. 102 (2013) 1–5.

[34] G. Sernicola, T. Giovannini, P. Patel, J.R. Kermode, D.S. Balint, T. Ben Britton, F. Giuliani, In situ stable crack growth at the micron scale, Nat. Commun. 8 (2017).

[35] F.W. DelRio, S.J. Grutzik, W.M. Mook, S.M. Dickens, P.G. Kotula, E.D. Hintsala, D. D. Stauffer, B.L. Boyce, Eliciting stable nanoscale fracture in single-crystal silicon, Mater. Res. Lett. 10 (11) (2022) 728–735.

[36] B.N. Jaya, C. Kirchlechner, G. Dehm, Can microscale fracture tests provide reliable fracture toughness values? A case study in silicon, J. Mater. Res. 30 (5) (2015) 686–698.

[37] Dassault Systèmes Simulia Corp., Abaqus Analysis User's Manual Volume II: Analysis, Version 6.12. 2 (2012) 831

[38] S. Brinckmann, K. Matoy, C. Kirchlechner, G. Dehm, On the influence of microcantilever pre-crack geometries on the apparent fracture toughness of brittle materials, Acta Mater. 136 (2017) 281–287.

[39] H. Gopalan, A. Marshal, M. Hans, D. Primetzhofer, N. Cautaerts, B. Breitbach, B. Völker, C. Kirchlechner, J.M. Schneider, G. Dehm, On the interplay between microstructure, residual stress and fracture toughness of (Hf-Nb-Ta-Zr)C multi-metal carbide hard coatings, Mater. Des. 224 (2022) 111323.

[40] A.R. Boccaccini, R.D. Rawlings, I. Dlouhý, Reliability of the chevron-notch technique for fracture toughness determination in glass, Mater. Sci. Eng. A 347 (1-2) (2003) 102–108.

[41] M.G. Mueller, G. Žagar, A. Mortensen, Stable room-temperature micron-scale crack growth in single-crystalline silicon, J. Mater. Res. 32 (19) (2017) 3617–3626.

[42] H.W. Andresen, A.T. Echtermeyer, Critical energy release rate for a CSM reinforced carbon fibre composite/steel bonding, Compos. A Appl. Sci. Manuf. 37 (5) (2006) 742–751.

[43] J.M. Whitney, C.E. Browning, W. Hoogsteden, Double Cantilever Beam Tests for Characterizing Mode I Delamination of Composite Materials, J. Reinf. Plast. Compos. 1 (1982) 297–313.

[44] T.L. Anderson, Fracture Mechanics: Fundamentals and Applications, Third, Taylor & Francis, 2005

[45] Y.-W. Mai, B.R. Lawn, Crack Stability and Toughness Characteristics in Brittle Materials, Annu. Rev. Mater. Sci. 16 (1) (1986) 415–439.

[46] B. Lawn (Ed.), Fracture of Brittle Solids, Cambridge University Press, 1993.

[47] B.N. Jaya, S. Bhowmick, S.A.S. Asif, O.L. Warren, V. Jayaram, Optimization of clamped beam geometry for fracture toughness testing of micron-scale samples, Phil. Mag. 95 (16-18) (2015) 1945–1966.

[48] C. Gee, J.N. Weddell, M.V. Swain, Comparison of three and four point bending evaluation of two adhesive bonding systems for glass-ceramic zirconia bi-layered ceramics, Dent. Mater. 33 (9) (2017) 1004–1011.

[49] J.L. Mead, M. Lu, H. Huang, Microscale interfacial adhesion assessment in a multilayer by a miniaturised four-point bending test, Mech. Mater. 129 (2019) 341–351.

[50] L. Banks-Sills, 50th anniversary article: Review on interface fracture and delamination of composites, Strain 50 (2014) 98–110.

[51] R. Krueger, K. Shivakumar, I.S. Raju, Fracture mechanics analyses for interface crack problems a review, 54th AIAA/ASME/ASCE/AHS/ASC Struct. Struct. Dyn. Mater. Conf. (2013).

[52] A. Agrawal, A.M. Karlsson, Obtaining mode mixity for a bimaterial interface crack using the virtual crack closure technique, Int. J. Fract. 141 (1-2) (2006) 75–98.

[53] M. Charalambides, A.J. Kinloch, Y. Wang, J.G. Williams, On the analysis of mixed-mode failure, Int. J. Fract. 54 (3) (1992) 269–291.

[54] J.W. Hutchinson, Adv. Appl. Mech. 16 (1976) 1976.

[55] R.O. Ritchie, R.M. Cannon, B.J. Dalgleish, R.H. Dauskardt, J.M. McNaney, Mechanics and mechanisms of crack growth at or near ceramic-metal interfaces: interface engineering strategies for promoting toughness, Mater. Sci. Eng. A 166 (1-2) (1993) 221–235.

[56] V. Stamos, V. Kostopoulos, S.D. Peteves, Fracture Criteria for Interface Cracks A Case Study, Interfacial Sci. Ceram. Join. (1998) 267–279.

[57] H.e. Ming-Yuan, J.W. Hutchinson, Crack deflection at an interface between dissimilar elastic materials, Int. J. Solids Struct. 25 (9) (1989) 1053–1067.

[58] Q.H. Qin, X. Zhang, Crack deflection at an interface between dissimilar piezoelectric materials, Int. J. Fract. 102 (2000) 355–370.

[59] D. Picard, D. Leguillon, C. Putot, A method to estimate the influence of the notch-root radius on the fracture toughness measurement of ceramics, J. Eur. Ceram. Soc. 26 (8) (2006) 1421–1427.

[60] H. Yu, G.B. Thompson, C.R. Weinberger, The role of chemistry and bonding in regulating fracture in multiphase transition metal carbides and nitrides, Extrem. Mech. Lett. 17 (2017) 1–6.

[61] J.A. Hauch, D. Holland, M.P. Marder, H.L. Swinney, Dynamic fracture in single crystal silicon, Phys. Rev. Lett. 82 (19) (1999) 3823–3826.

[62] R. Pérez, P. Gumbsch, Directional anisotropy in the cleavage fracture of silicon, Phys. Rev. Lett. 84 (23) (2000) 5347–5350.

[63] A. Gleizer, D. Sherman, The cleavage energy at initiation of (110) silicon, Int. J. Fract. 187 (1) (2014) 1–14.

[64] S.B. Bhaduri, F.F.Y. Wang, Fracture surface energy determination in {1 1 0} planes in silicon by the double torsion method, J. Mater. Sci. 21 (1986) 2489–2492.

[65] A.A. Stekolnikov, J. Furthmüller, F. Bechstedt, Absolute surface energies of group-IV semiconductors: Dependence on orientation and reconstruction, Phys. Rev. B –– Condens. Matter Mater. Phys. 65 (2002) 1–10.

[66] J.C.H. Spence, Y.M. Huang, O. Sankey, Lattice trapping and surface reconstruction for silicon cleavage on (111). Ab-initio quantum molecular dynamics calculations, Acta Metall. Mater. 41 (10) (1993) 2815–2824.

[67] T. Rouxel, S. Yoshida, The fracture toughness of inorganic glasses, J. Am. Ceram. Soc. 100 (10) (2017) 4374–4396.